Theory of high-temperature photorefractive phenomena in LiNbO₃ crystals and applications to experiment

B. I. Sturman, M. Carrascosa, F. Agulló-López, and J. Limeres

Departamento Física de Materiales, C-IV, Universidad Autónoma de Madrid, Cantoblanco, Madrid, E-28049, Spain

(Received 19 November 1997)

We develop a theory of high-temperature photorefractive phenomena in LiNbO₃ crystals related to the problem of thermal fixing and storage of optical information. The theory covers the temperature range 20–300 °C relevant to the experiment. It is based on a systematic exploiting of small physical parameters, typical of the subject, and distinguished by general and simple expressions for characterization of the fixing, developing, and decay processes. It is shown that thermally excited electrons are competitive with protons (responsible for the charge compensation) within a wide high-temperature region 200–300 °C. They are not only responsible for the dark decay of information, but also for pronounced high-temperature peculiarities of the recording and relaxation processes. A good qualitative agreement between the theory and a great amount of accumulated factual data are obtained. [S0163-1829(98)03920-4]

I. INTRODUCTION

Currently, after more than 20 years of development,[1–13] studies of high-temperature photorefractive phenomena related to the opical storage problem have experienced a remarkable upsurge.[14–34] Advances of experimental techniques, accumulated factual data and an experience in modeling of the relevant processes of charge transfer, have made it possible to approach a clear physical picture of the whole subject.

The above studies date back to the idea of how to make permanent the optical information recorded in a photorefractive crystal in the form of an electronic charge replica. It was proposed[1] that during high-temperature recording of information (a sinusoidal spatial grating, hologram, in the simplest case) or during the heating of the crystal with a previously recorded replica, the electronic charge may be compensated by optically passive thermally activated ions. Cooling the crystal to room temperature makes the ions immobile, and the corresponding ionic replica becomes permanent. First experiments on LiNbO₃ crystals supported this physical idea and demonstrated the potential of the thermal fixing technique.[2]

Main efforts have, so far, been focused on thermal fixing and relevant high-temperature photorefractive processes in LiNbO₃, which remains the most promising material for storage applications. It has been proved unambiguously[6,28] that the optically passive ions, responsible for the charge compensation, are protons. Many experiments have shown that the main mechanisms of electron charge transfer are drift and diffusion of photoexcited electrons and also the photovoltaic effect.[35,36] The last one is associated with the spatial asymmetry of photoionization in noncentrosymmetrical materials. Initial model equations incorporating the mentioned transport mechanisms are well known, as well as their general solutions in the limit of small contrast of the light pattern,[7,10,16,29] and they are not the subject of much controversy. The main stages of kinetic processes related to the fixing phenomenon are recognized fairly well.[7,16,29] An ap-

preciable amount of experimental data is accumulated on the subject.[8,9,13,15,20,23–25,29,30,33,34]

Figure 1(a) illustrates a typical temporal dependence of the amplitude of the space-charge field (which is one of the most important measurable characteristic of the hologram) during the process of high-temperature recording and the subsequent development or (and) decay. It corresponds to the recording temperature $T=160-180$ °C usual for the thermal fixing. Many features of the depicted processes, in particular the presence of fast and slow stages of recording and decay, are understood nowadays. It is worth noting that a considerable progress in theory and experiment has been made in the last few years. So only recently was the slow stage of the dark decay associated with thermal excitation of electrons.[29]

In spite of the progress made, the physical picture of fixing-related phenomena in LiNbO₃ remains incomplete and fragmental. On the one hand, systematization of experimental data has been hampered by the instability of the interference light fringes during recording and bad control of the crystal parameters. On the other hand, theoretical works have been, so far, unable to provide experiments with a sufficient set of predictions concerning the main features of fixing-related phenomena. Such important questions as what the optimum conditions are for the fixing procedure within the accepted model and how the characteristics of developing and decay depend on the recording time have not been satisfactorily answered. Conflicting statements persist about the storage time of a fixed hologram.[32,33] Surprisingly little attention has been paid to a comparison of the theoretical predictions with accumulated experimental data. Moreover, drastic qualitative changes in the photorefractive behavior of LiNbO₃ crystals above 200 °C depicted in Fig. 1(b) remain unclear, although the implication of thermal electrons in these changes has been suggested.[17]

In this paper we try to fill the gap in theoretical studies of high-temperature photorefractive effects in LiNbO₃ and to establish a bridge between theory and available factual data. A distinctive feature of our approach is a systematic exploiting of small parameters relevant to the subject that allows us

to simplify the analytical expressions and make them physically meaningful. Figures serve us mainly for illustration of the established general dependences. In this way, we have described in a simple manner all the rate coefficients and the characteristic amplitudes for the recording and relaxation processes, as well as the impact of the fixing duration on the subsequent developing and decay. Inclusion of the high-temperature region, $T \gtrsim 200\,°C$, in our considerations has allowed to gain a insight into the role of thermal electrons in fixing-related phenomena and to reveal distinctive manifestations of these carriers.

The structure of the paper is as follows. Section II forms the theoretical basis. We discuss first the structure of the initial set of coupled equations for the space-charge field and the concentrations of protons, electrons, and ionized traps. Then we introduce the main approximations to arrive at simplified equations for the amplitudes of electronic and protonic gratings induced by a periodic light pattern. Having a very simple structure, these equations incorporate the essence of the high-temperature photorefractive phenomena. Further, on the basis of the literature data, we analyze the values and the temperature dependences of the parameters entering the simplified equations and make numerical estimates to justify the approximations made.

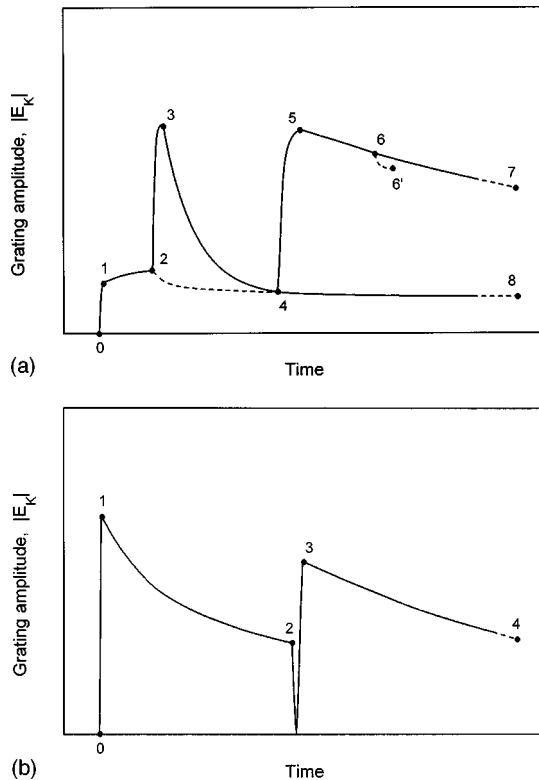In Sec. III we describe the slow and fast relaxation modes

FIG. 1. Two typical life histories of holograms in LiNbO$_3$. (a) $T \lesssim 180\,°C$. The segments 0–1 and 1–2 depict the f and s recording stages, 2–3 and 4–5 correspond to the developing process, 2–4 and 3–4 to the f stage of dark decay, 5–7 to the light-induced decay, and 4–8 to the s stage of dark decay. The segment 6–6' illustrates the increasing rate of decay after switching off the light. (b) $T > 220\,°C$. The segments 0–1 and 1–2 correspond to the f and s stages of recording, 2–3 to the f stage of relaxation at the same temperature, and 3–4 to the s stage of relaxation.

on the basis of the simplified equations. This includes the relaxation rates and the relationships between the amplitudes of electronic and ionic gratings (eigenvalues and eigenvectors). We show that the slow relaxation mode is responsible for charge compensation, which is at the heart of the fixing-related phenomena. Last, we consider actual limiting cases for the relaxation rates.

Section IV is devoted to the characterization of the two-stage recording process. We show that the inclusion of thermal electrons into consideration changes dramatically the high-temperature behavior and allows us to explain peculiarities of the experimental photorefractive kinetics above $200\,°C$. We demonstrate also that the slow stage of recording, during which the changes of the space-charge field are not pronounced, is of prime importance for fixing during recording.

In Sec. V we analyze different relaxation processes following high-temperature recording. First, it is shown in a general form that the characteristic amplitude of the space-charge field, which is achieved after the fast stage of a certain relaxation process, depends essentially on the duration of the original recording stage, but not on the history of the intermediate fast relaxations. We derive further explicit expressions for the space-charge field amplitude characterizing the processes of developing and decay at different temperatures. We demonstrate that thermally excited electrons manifest themselves clearly in the high-temperature relaxation processes.

In the final sections, Secs. VI and VII, we discuss the findings and applications of our studies, and formulate the conclusions.

II. THEORETICAL BACKGROUND

A. Initial equations

Our theoretical studies are based on the conventional two-species model for the thermal fixing.[10,16,29] It is supposed that the charge carriers are protons and free electrons. The electrons may be excited optically and thermally from deep immobile traps of only one kind. The above excitation processes are balanced by a recombination of electrons to the empty traps. The transport processes for H$^+$ ions are drift in the space-charge field and diffusion. For electrons we take additionally into account photovoltaic transport owing to the asymmetry of the photoexcitation.[35,36] This is especially important for LiNbO$_3$ crystals doped with Fe and Cu.

The buildup of the space-charge field (hologram) is supposed to be induced by the spatial modulation of the light intensity, $I = I_0(1 + m \cos Kz)$, where m is the contrast of the light pattern and K the grating vector. Relaxation processes may occur either under uniform illumination ($m = 0$) or in the dark.

The dynamic variables in our model are the space-charge field E, the density of free electrons n, the concentration of ionized traps N^+, and the hydrogen concentration H. These variables obey the following coupled set of electrostatics and rate equations:

$$\frac{\partial E}{\partial z} = \frac{e}{\epsilon\epsilon_0}(N^+ - N_A + H - H_0 - n),$$

$$\frac{\partial N^+}{\partial t} = (S_T + S_{ph}I)(N - N^+) - S_r N^+ n,$$

$$\frac{\partial n}{\partial t} = \frac{\partial N^+}{\partial t} + \frac{1}{e}\frac{\partial j_e}{\partial z},$$

$$\frac{\partial H}{\partial t} = -\frac{1}{e}\frac{\partial j_h}{\partial z}. \tag{1}$$

Here e is the absolute value of the electron charge, $\epsilon\epsilon_0$ the dielectric constant, H_0 the average hydrogen concentration, N the total trap concentration, N_A the concentration of compensating passive acceptors, and S_T, S_{ph}, and S_r are microscopic parameters characterizing the processes of thermal excitation, photoionization, and recombination, respectively. The current densities j_e and j_h, related to electrons and protons, are given by

$$j_e = e\mu_e n E + eD_e\frac{\partial n}{\partial z} + \beta(N - N^+)I,$$

$$j_h = e\mu_h H E - eD_h\frac{\partial H}{z}, \tag{2}$$

where $\mu_{e,h}$ are the mobilities of electrons and H$^+$ ions, $D_{e,h}$ their diffusion coefficients, and β is the photovoltaic coefficient. In accordance with Einstein relation, we have $D_{e,h} = \mu_{e,h}k_BT/e$, where k_B is Boltzmann constant and T the absolute temperature.

It is assumed in Eqs. (2) that the electric field inside the crystal has no spatially uniform component. The motivation for this physical restriction will be given below in this section. Mathematically, the above assumption means that the spatial average of the space-charge field, $\langle E \rangle$, is zero. We suppose also that the crystal is neutral as a whole. This means that the spatial average $\langle N^+ - N_A + H - H_0 - n \rangle$ is zero.

It is important to take into account that in all actual cases the concentration of free electrons is much less than the concentrations of filled and empty traps. This means, in particular, that the thermal and photoexcitations affect the uniform parts of N^+ and $N - N^+$ negligibly. Below in this section we provide the reader with numerical estimates justifying this assumption. The spatial averages $N_A = \langle N^+ \rangle$ and $N_D = \langle N - N^+ \rangle$, i.e., the concentrations of acceptors and donors, are important characteristics of the crystal. For LiNbO$_3$ usually $N_D \ll N_A$.[30,37]

Now we can introduce a number of important physical parameters characterizing the electron processes proceeding under uniform illumination. These parameters are the electron lifetime $\tau_e = (S_r N_A)^{-1}$, the light absorption coefficient $\alpha = S_{ph}N_D\hbar\omega$, where $\hbar\omega$ is the energy of a light quantum, the rates of thermal (T) and photo (ph) excitations, $g^T = S_T N_D$ and $g^{ph} = \alpha I_0/\hbar\omega$, the total rate of excitation, $g_0 = g^T + g^{ph}$, the average electron concentration $n_0 = g_0\tau_e$, which consists of the thermal and photonic parts; and last, the photovoltaic field $E_{PV} = \beta I_0 N_D/e\mu_e n_0^{ph}$

$= \beta S_r N_A/e\mu_e S_{ph}$. Note that the product $e\mu_e n_0^{ph}$ is the photoconductivity, the product $e\mu_e n_0^T$ is the electron contribution to the dark conductivity, and the combination $\beta N_D I_0$ is the direct photovoltaic current measurable in experiment. In many cases the parameters α, $\mu_e\tau_e$, E_{PV}, and βN_D may be found experimentally. It is useful also to introduce the dielectric relaxation rates related to electrons and protons, γ_e and γ_h. They are given by

$$\gamma_e = e\mu_e n_0/\epsilon\epsilon_0, \quad \gamma_h = e\mu_h H_0/\epsilon\epsilon_0. \tag{3}$$

In accordance with the above expression for g_0, the electronic rate γ_e consists of the thermal (γ_e^T) and photo (γ_e^{ph}) contributions. The sum $\gamma = \gamma_e + \gamma_h$ is the overall rate of dielectric relaxation. Its inverse γ^{-1} is the characteristic relaxation time of a macroscopic electric field due to the electric conduction.

B. Simplified equations

Our aim is to describe the response of the crystal to the spatially modulated light intensity. In this way we shall use a number of approximations exploiting the smallness of certain physical parameters entering the initial equations (1) and (2). At the first step we assume the following conventional approximations.[7,10,16,29]

(i) Linear approximation in the contrast m. The higher Fourier harmonics of the dynamic variables are supposed to be negligible in comparison with the fundamental components. This means a representation of the variables in the form

$$E = E_K e^{iKz} + \text{c.c.},$$

$$N^+ - N_A = N_K^+ e^{iKz} + \text{c.c.},$$

$$H - H_0 = H_K e^{iKz} + \text{c.c.},$$

$$n - n_0 = n_K e^{iKz} + \text{c.c.}, \tag{4}$$

where "c.c." means the complex conjugate. In general, neglect of higher harmonics imposes some restriction on the contrast m.

(ii) The temporal derivative $\partial n_K/\partial t$ in the third equation of the set (1) is negligible in comparison with the term n_K/τ_e coming from the right-hand side of this equation. This so-called adiabatic approximation exploits the smallness of the electron lifetime as compared with the characteristic relaxation times. Usually, this requirement is fulfilled with a large margin of safety.

(iii) The amplitude n_K appearing in the first of Eqs. (1) is negligible in comparison with the amplitudes N_K^+ and H_K. This approximation is also well justified since it also makes use of the smallness of the electron lifetime.

Under these approximations we obtain from Eqs. (1) and (2) the following closed linear set of evolution equations for the amplitudes N_K^+ and H_K:

$$\frac{dN_K^+}{dt} + \widetilde{\gamma}_e(1+\xi_e)N_K^+ + \widetilde{\gamma}_e H_K = F_K,$$

$$\frac{dH_K}{dt} + \gamma_h N_K^+ + \gamma_h(1+\xi_h)H_K = 0. \tag{5}$$

Here γ_h is the protonic rate of the dielectric relaxation, introduced earlier, and $\widetilde{\gamma}_e = \gamma_e(1+K^2L_D^2)^{-1}$ is the renormalized electronic rate with the electron diffusion length $L_D = (D_e\tau_e)^{1/2}$. The dimensionless parameters $\xi_{e,h}$ and the effective driving force F_K, entering Eqs. (5), are given by

$$\xi_e = \frac{E_D}{E_q} - i\,\frac{E_{PV}}{E_q}\frac{N_A}{N}\frac{\gamma_e^{ph}}{\gamma_e},$$

$$\xi_h = \frac{E_D}{E_q}\frac{N_t}{H_0},$$

$$F_K = -i\,\frac{m}{2}\,N_t\gamma_e^{ph}\frac{E_{PV}+iE_D}{E_q}, \tag{6}$$

where $E_D = Kk_BT/e$ and $E_q = eN_t/\epsilon_0\epsilon K$ are so-called diffusion and saturation fields, and $N_t = N_AN_D/N$ is the effective trap concentration. The introduced notation is conventional for the photorefractive area.[38]

With the last of the above approximations, the field amplitude E_K is expressed algebraically by the sum $N_K^+ + H_K$:

$$E_K = -iE_q\,\frac{N_K^+ + H_K}{N_t}. \tag{7}$$

Note that the value of $|E_K|$ may be measured directly by means of Bragg diffraction of light from the refractive index grating linked with the grating of the space-charge field via the linear electro-optic effect. This is why the variable E_K is of prime importance in our theory.

The structure of the system (5) is worthy of attention. It is seen that the protonic component is not driven directly, but only via the electronic one. This is due to the protons being optically passive. The renormalization of the dielectric relaxation rate related to electrons (i.e., the replacement of γ_e by $\widetilde{\gamma}_e$) does not affect the structure of the set (5). Furthermore, this renormalization is always very small. In what follows, we ignore the difference between $\widetilde{\gamma}_e$ and γ_e in Eqs. (5).

The dimensionless parameters $\xi_{e,h}$ are small in most actual cases, $|\xi_e|, \xi_h \ll 1$. The terms including these parameters are, however, indispensible in the governing system (5) because they form its structure. It is obvious, in particular, that Eqs. (5) have no stationary solutions if the parameters $\xi_{e,h}$ are omitted. One can say in advance that the smallness of $\xi_{e,h}$ predetermines many essential features of high-temperature photorefractive phenomena.

The parameter ξ_e is generally complex; its imaginary part is due to the photovoltaic effect. As was mentioned, in LiNbO$_3$ crystals we have $N_D \ll N$ so that $N \simeq N_A$; in what follows, we put for simplicity $N_A/N = 1$ in the relation (6) for ξ_e. The expressions for ξ_e and F_K both come from diffusion and photovoltaic contributions. The photovoltaic share in ξ_e and F_K is, however, different. The driving force F_K is proportional to the effective driving field $E_{eff}=E_{PV}$
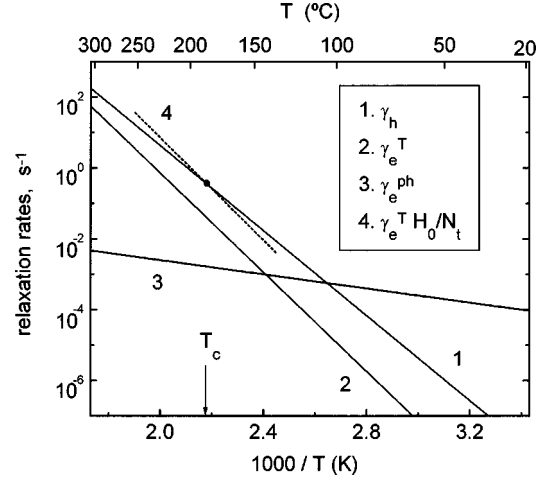

FIG. 2. Arrhenius plots for the dielectric relaxation rates (solid lines) and for the ratio $\gamma_e^T H_0/N_t$ (dashed line).

$+iE_D$, whereas the ξ_e factor is proportional to $E_{PV}\gamma_e^{ph}\gamma_e^{-1}$ $+iE_D$. This distinction is important for high-temperature photorefractive phenomena.

Our subsequent considerations are based on the simplified evolution equations (5) and the relations (6) and (7). At the same time, the temperature dependences of the rate coefficients γ_h, γ_e^{ph}, and γ_e^T, entering the basic equations, carry a great deal of additional information on the high-temperature recording and relaxation processes.

C. Material parameters

Fixing-related phenomena deal with a considerable number of material parameters. Some of them are known fairly well, whereas information about some others is very scanty. On the other hand, relations between the material parameters essentially define the character of high-temperature photorefractive effects.

It is well established nowadays that hydrogen ions H$^+$ are responsible for the compensation of the electronic charge in LiNbO$_3$ crystals.[6,28] The concentration of hydrogen, H_0, varies usually from $\sim 10^{18}$ to $\sim 10^{19}$ cm^{-3}. The temperature dependence of the mobility μ_h has been investigated in a number of experimental papers; see, e.g., Refs. 14 and 28. It obeys an activation law $\mu_h = \mu_h^0\exp(-\varepsilon_h/k_BT)$, typical for hopping ion motion. The activation energy ε_h in LiNbO$_3$ crystals varies usually from 1.1 to 1.3 eV; in the case of Fe-doped samples, $\varepsilon_h \simeq 1.2$ eV. The preexponential mobility factor μ_h^0 is expressed as $\mu_h^0 = eD_h^0/k_BT$ with a virtually constant preexponential diffusivity factor D_h^0; according to the literature data, D_h^0 ranges from $\sim 10^{-1}$ to ~ 1 cm^2/s in bulk crystals.[14,28]

The above data allow us to estimate the temperature dependence of the ionic relaxation rate γ_h. Line 1 in Fig. 2 is the Arrhenius plot of γ_h for $H_0 = 3\times10^{18}$ cm^{-3}, $\varepsilon_h = 1.2$ eV, $D_h^0 = 0.3$ cm^2/s, and the dielectric constant of LiNbO$_3$, $\epsilon = 30$. It is seen that within the temperature interval 50–300 °C the rate γ_h ranges from $\sim 10^{-6}$ to $\sim 10^2$ s^{-1}.

Concerning the electron transport, the accepted one-trap model is well justified for LiNbO$_3$ crystals doped with Fe or Cu.[37,39] In the first case, the ions Fe^{2+} and Fe^{3+} serve as

donors and acceptors, respectively. For Cu-doped crystals these are Cu^+ and Cu^{2+}. In both cases one can accept usually that $N_D \ll N$. The effective trap concentration $N_t \simeq N_D$ is typically of the order of 10^{18} cm^{-3}; i.e., it is either comparable or less than the hydrogen concentration H_0. Increasing N_D results in an undesirably strong light absorption, whereas decreasing N_D to $\sim 10^{17}$ cm^{-3} makes the accepted model hardly reliable because of uncontrollable defects present in LiNbO$_3$.

The photoelectric properties of LiNbO$_3$ crystals have been mostly investigated at room temperature.[36] It is established that the photovoltaic transport dominates for Fe- or Cu-doped samples. The photovoltaic constant may be estimated as $\beta \approx 0.5 \times 10^{-26}$ cm^3/V. The product $\mu_e \tau_e$ ranges usually from $\sim 10^{-12}$ to $\sim 10^{-13}$ cm^2/V; correspondingly, the photovoltaic field E_{PV} varies from $\sim 10^1$ to $\sim 10^2$ kV/cm. In spite of rather low values of the $\mu_e \tau_e$ product, the photoconductivity at room temperature dominates over the dark conductivity already for very low laser intensity (<1 mW/cm^2). For light intensity $I_0 \sim 10^{-1}$ W/cm^2, typical for cw experiments, the dielectric relaxation rate $\gamma_e^{ph} \approx 10^{-2}$–$10^{-3}$ s^{-1}.

The temperature dependence of the photovoltaic constant β, as well as of the light absorption coefficient α, is rather weak. At the same time, according to Refs. 36 and 40, the photoconductivity (i.e., the $\mu_e \tau_e$ product) is thermally activated with an activation energy $\varepsilon_e^{ph} \approx 0.16$ eV. Similar information may be extracted from the experimental data of Ref. 13. Note that a temperature dependence of the photoconductivity with an activation energy $\varepsilon_e^{ph} = 0.1$–0.3 eV seems to be typical for many ferroelectrics.[41] Usually, it is explained by the thermally assisted small polaron conduction.[37,39] An alternative mechanism is associated with the spatial modulation of the bottom of the conductivity band.[42] The microscopic mechanism of the thermally activated photoconductivity is irrelevant for the purpose of our studies.

Line 2 in Fig. 2 shows a representative temperature dependence of γ_e^{ph}. We have taken $\varepsilon_e^{ph} = 0.15$ eV and chosen a reasonable experimental value of γ_e^{ph} for room temperature. One sees that increasing the temperature from 20 to 200 °C increases γ_e^{ph} (and, consequently, decreases E_{PV}) by approximately one order of magnitude.

Direct measurements of the electron mobility are hampered by its low value. One can expect that for room temperature $\mu_e \lesssim 10^{-2}$ cm^2/V s. The electron lifetime, which corresponds to this estimate, is of the order of 10^{-10} s.

Very little is known about the electron component of the dark conductivity, $e\mu_e n_0^T = e\mu_e \tau_e S_T N_D$, for LiNbO$_3$ crystals. One can say with a fair degree of confidence that within the temperature interval 20–200 °C this component does not exceed the conductivity of H$^+$ ions. It is clear from general considerations that the thermal electronic conductivity is thermally activated. The corresponding activation energy ε_e^T consists of two contributions related to the rate of thermal excitation of electrons from deep traps S_T and to the $\mu_e \tau_e$ product, respectively. One can expect that the first contribution can hardly be less than 1 eV. So we can accept that the rate γ_e^T, related to thermal electrons, is proportional to $\exp(-\varepsilon_e^T / k_B T)$ with $\varepsilon_e^T > 1$ eV.

We shall see in what follows that the thermal electronic contribution is of prime importance for the high-temperature domain. Line 3 in Fig. 2 shows a representative dependence $\gamma_e^T(T)$. It has been chosen to explain a great body of accumulated experimental data on the kinetics of the high-temperature recording and relaxation processes in LiNbO$_3$; see Secs. IV and V. The value taken of the activation energy is $\varepsilon_e^T = 1.4$ eV. Within the whole temperature interval, the thermal component of the electronic conductivity is small in comparison with the protonic conductivity.

D. Numerical estimates

The above information and assumptions on the relevant material parameters enables us to make a number of numerical estimates to justify the approximations made earlier and to gain an overall view of the subject.

Let us estimate first the characteristic diffusion and saturation fields $E_D = K k_B T/e$ and $E_q = e N_t/\epsilon \epsilon_0 K$, which do not experience strong temperature dependences. Setting $\epsilon = 30$, $T = 200$ °C, $N_t = 5 \times 10^{17}$ cm^{-3}, and the grating spacing $\Lambda \equiv 2\pi/K = 1$ μm, we obtain $E_D \simeq 2.5$ kV/cm and $E_q \simeq 500$ kV/cm. At this temperature the photovoltaic field E_{PV} ranges presumably between 10^0 and 10^1 kV/cm; roughly, it is comparable with E_D. The ratio E_D/E_q equals $K^2 R_d^2$, where $R_d = (\epsilon \epsilon_0 k_B T/N_t e^2)^{1/2}$ is the Debye screening length. According to our estimates for E_D and E_q, we have $K^2 R_d^2 \approx 10^{-2}$.

The electron diffusion length $L_D = (D_e \tau_e)^{1/2}$ may be estimated using the data on the $\mu_e \tau_e$ product. Assuming $\mu_e \tau_e = 10^{-12}$ cm^2/V, we get $L_D \simeq 20$ Å for 200 °C. Because of the square root law, this estimate is not very sensitive to variations of the $\mu_e \tau_e$ product and T. The characteristic photovoltaic drift length $L_{PV} = \mu_e \tau_e E_{PV}$ is typically less than 1 Å.

To justify the neglect of the derivative $\partial n/\partial t$ in Eqs. (1), one should make certain that the lifetime τ_e is much shorter than the relaxation time γ^{-1}. For the accepted values of crystal parameters and the data of Fig. 2, we obtain $\gamma \tau_e \lesssim 10^{-8}$. So the above adiabatic approximation is justified perfectly well.

Our neglect of n_K in comparison with N_K^+ and H_K in the first of Eqs. (1) also implies the smallness of τ_e. To estimate roughly the ratio n_K/N_K^+, it is sufficient to notice that $n_K \lesssim g_0 \tau_e$ and to take that the space-charge amplitude $e N_K^+$ corresponds to the characteristic field E_D. For the light intensity $I_0 \lesssim 1$ W/cm^2 and the accepted values of crystal parameters, the ratio n_K/N_K^+ does not exceed 10^{-5}.

The renormalization of the electronic relaxation rate in Eqs. (5) is negligible when $K^2 L_D^2 \ll 1$. Since $L_D \sim 10^1$ Å, this inequality is fulfilled perfectly well even for a grating spacing Λ comparable with the light wavelength.

Neglect of the higher Fourier harmonics of the dynamic variables (the linear approximation in the contrast m) has generally no strong safety margin. It should be understood, however, that allowance for higher harmonics cannot change the structure of the left-hand side of the simplified equations (5), which, actually, is the fingerprint of the theory of high-temperature photorefractive processes. Corrections for higher harmonics could merely give a renormalization of the driv-

ing force F_K in the right-hand side of Eqs. (5). As long as $H_0 \gtrsim N_t$, this renormalization is numerically small even for $m \simeq 1$. Anyway, decreasing m suppresses strongly the effect of higher harmonics.

The assumption of a zero uniform component of the electric field, made in Sec. II A, may be justified as follows. If the photovoltaic effect is negligible, $E_{PV} \ll E_D$, this assumption corresponds to the case of zero applied voltage. If we have $E_{PV} \gtrsim E_D$, it corresponds to the so-called closed circuit regime, which provides for optimum conditions for photovoltaic charge separation and, furthermore, is most typical for experiment.[29,36] The role of the photovoltaic field E_{PV} is similar here to the role of a strong applied field. In such a way, the above assumption incorporates most actual situations for experiments with $LiNbO_3$ crystals.

Finally, let us estimate the values of dimensionless parameters $\xi_{e,h}$ entering the simplified equations (5). For $N_t = 5 \times 10^{17}$ cm^{-3}, $\Lambda = 1$ μm, and $T = 200$ °C, we have, in accordance with the previous estimates, $\xi'_e \equiv \mathrm{Re}\,\xi_e \simeq 5 \times 10^{-3}$. Only for an extremely small effective trap concentration $N_t \lesssim 10^{17}$ cm^{-3} and very small grating spacing $\Lambda \ll 1$ μm may the real part of ξ_e approach 1. The value of $\xi''_e \equiv \mathrm{Im}\,\xi_e$ is strongly dependent on the temperature. In the region of sufficiently low temperature, where $\gamma_e^{ph} \gtrsim \gamma_e^T$, we have $\xi''_e \gtrsim \xi'_e$. Increasing T results in a decrease of E_{PV} and, what is more important, in a sharp decrease of the ratio γ_e^{ph}/γ_e^T; see also Fig. 2. For this reason, in the high-temperature domain, where $\gamma_e^{ph} \ll \gamma_e^T$, the parameter ξ_e is nearly real, $\xi''_e \ll \xi'_e$.

The dimensionless parameter ξ_h is always real. Since $N_t \lesssim H_0$, we have $\xi_h \ll 1$ even with a larger safety margin than for ξ'_e.

III. FAST AND SLOW RELAXATION MODES

Within the approximations made in the previous section, the dynamic variables have only two degrees of freedom and they are governed by the second-order linear equations (5). This linear set may be characterized by two relaxation modes (fast and slow) and, correspondingly, by two relaxation rates Γ_f and Γ_s.[7,10,29,31] To find these rates, we put $F_K = 0$ and N_K^+, $H_K \propto \exp(-\Gamma t)$ in Eqs. (5). After that we arrive at the following algebraic system for N_K^+ and H_K:

$$[-\Gamma + \gamma_e(1 + \xi_e)]N_K^+ + \gamma_e H_K = 0,$$

$$\gamma_h N_K^+ + [-\Gamma + \gamma_h(1 + \xi_h)]H_K = 0. \tag{8}$$

The condition of solvability of this system gives us two solutions for the rate Γ. Since $|\xi_{e,h}| \ll 1$, it is sufficient to find these solutions in the leading approximations in $\xi_{e,h}$. After simple calculations we obtain

$$\Gamma_f = \gamma_e + \gamma_h, \quad \Gamma_s = \frac{\gamma_e \gamma_h}{\gamma_e + \gamma_h}(\xi_e + \xi_h). \tag{9}$$

These expressions include a great deal of information about fast (f) and slow (s) relaxation processes. The fast rate Γ_f is simply the overall rate of the dielectric relaxation γ. The smallness of the slow rate in comparison with the fast one

comes from both factors entering expression (9) for Γ_s. Putting γ_e or γ_h equal to zero in this expression turns Γ_s to zero.

The slow rate is generally complex. Its real part Γ'_s, proportional to $K^2 R_d^2$, characterizes the ambipolar diffusion of electrons and protons. This diffusion is slowed down because of the electrostatic attraction of the opposite charges. The imaginary part Γ'' is due to the photovoltaic effect.

To analyze the temperature behavior of $\Gamma_{f,s}$, we consider separately the cases of dark ($I_0 = 0$) and light-induced ($I_0 \neq 0$) relaxations. The light-induced relaxation may be related to the transient recording stage and also to developing or decay of a recorded grating under uniform illumination.

Let, first, $I_0 = 0$. In this case we have $\gamma_e = \gamma_e^T$ and $\Gamma''_s = 0$. Within the temperature range where $\gamma_h \gg \gamma_e^T$ (in Fig. 2 this is, actually, the whole region), we obtain, from Eqs. (9),

$$\Gamma_f \simeq \gamma_h, \quad \Gamma_s \simeq \gamma_e^T K^2 R_d^2 (1 + N_t/H_0). \tag{10}$$

The temperature dependences of Γ_f and Γ_s are obviously thermally activated and characterized by the activation energies ε_h and ε_e^T, respectively.

Let now $I_0 \neq 0$. In this case, two temperature regions are of main interest. In the high-temperature limit, where $\gamma_h \gg \gamma_e^T \gg \gamma_e^{ph}$ (in Fig. 2 it corresponds to $T \gtrsim 160$ °C), the imaginary part of Γ_s is negligible and $\Gamma_{f,s}$ are given again by Eqs. (10). In the low-temperature limit, where $\gamma_e^{ph} \gg \gamma_h, \gamma_e^T$ (it corresponds to $T \lesssim 80$ °C in Fig. 2), we obtain

$$\Gamma_f \simeq \gamma_e^{ph}, \quad \Gamma'_s \simeq \gamma_h K^2 R_d^2 (1 + N_t/H_0),$$

$$\Gamma''_s \simeq -K\mu_h E_{PV} H_0/N_t. \tag{11}$$

The temperature dependences of Γ_f, Γ'_s and Γ''_s are characterized by the activation energies ε_e^{ph}, ε_h, and $\varepsilon_h - \varepsilon_e^{ph}$, respectively. It is likely that in this limit we have $|\Gamma''_s| \gg \Gamma'_s$. This means that instead of the relaxation s mode one should speak of a weakly damped propagating space-charge wave with eigenfrequency $-\Gamma''_s$. The presence of such an eigenmode may, as known, result in interesting resonance phenomena when the crystal is exposed to a running light pattern instead of a standing one.[43,44] Unfortunately, the low values of the eigenfrequency hamper the performance of resonance experiments.

Figure 3 shows the temperature dependences of Γ_f, Γ'_s, and Γ''_s, in the dark and under illumination, within the whole interval $20 \leq T \leq 300$ °C. It is assumed that the grating spacing $\Lambda = 1$ μm, $N_t = 5 \times 10^{17}$ cm^{-3}, $H_0 = 3 \times 10^{18}$ cm^{-3}, and $E_{PV}(20 \,°C) = 60$ kV/cm; the values of γ_h, γ_e^T, and γ_e^{ph} correspond to Fig. 2. It is seen that the value of Γ'_s is not practically affected by light. The imaginary part of Γ_s, related to the photovoltaic effect, is nonzero only under illumination. In the low-temperature region, where $\gamma_e^{ph} \gg \gamma_e^T, \gamma_h$, the ratio Γ_f/Γ'_s is strongly increasing with temperature.

It is possible that for short grating spacings ($\Lambda \ll 1$ μm) and a small effective trap concentration ($N_t \lesssim 10^{17}$ cm^{-3}) the photovoltaic field E_{PV} becomes comparable with E_q in the low-temperature limit. In this special case, the expression (11) for Γ'_s has to be replaced by
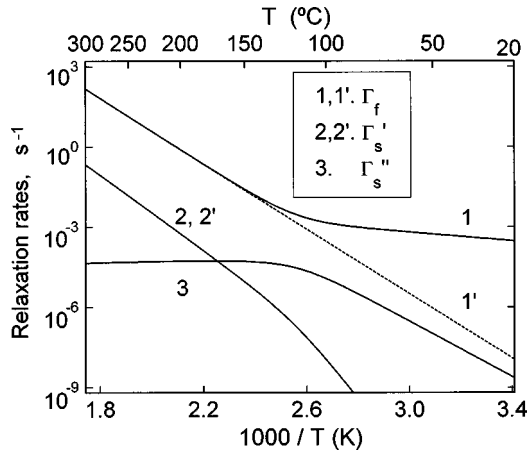
FIG. 3. Temperature dependences of the fast and slow relaxation rates. Curves 1 and 1′ characterize the fast rate Γ_f under illumination and in the dark, respectively; the coinciding curves 2 and 2′ show the real part of the slow rate Γ'_s, irrespectively of illumination, and curve 3 corresponds to the imaginary part Γ''_s under illumination.

$$\Gamma'_s \simeq \frac{\gamma_h}{1+E_q^2/E_{PV}^2}. \tag{12}$$

It should be kept in mind, however, that the initial simple model for electrons can hardly be justified for N_t well below 10^{17} cm^{-3}.

The algebraic system (8) not only allows one to calculate $\Gamma_{f,s}$ but also to find out the relations between the amplitudes N_K^+ and H_K for the f and s modes. By combining any of Eqs. (8) with the explicit expressions (9) for Γ_f and Γ_s, we obtain

$$N_K^+ \gamma_h = H_K \gamma_e \quad (f \text{ mode}),$$

$$H_K = -(1+\xi_e\gamma_e/\gamma-\xi_h\gamma_h/\gamma)N_K^+ \simeq -N_K^+ \quad (s \text{ mode}). \tag{13}$$

Hence the fast relaxation brings the system quickly to a state with nearly complete compensation of positive and negative charges. As we shall see, the obtained information about the f and s modes is highly useful for dealing with high-temperature recording and relaxation processes.

Let us compare the above theoretical predictions with available experimental data. Direct observations of the fast and slow stages of the dark decay of a preliminary recorded grating and direct measurements of the relaxation rates $\Gamma_{f,s}$ were reported for the temperature interval 144–168 °C.[23,24] These measurements have shown that $\Gamma_f \gg \Gamma_s$ with the fast rate Γ_f practically independent of the grating spacing and the slow rate $\Gamma_s \propto K^2$. Both relaxation constants were thermally activated. The measured activation energies for the f and s processes were $\varepsilon_f \simeq 1.1$ eV and $\varepsilon_s \simeq 1.3$ eV, respectively. The smallest detected values of Γ_s were of the order of 10^{-5} s^{-1}. Similar experimental data were obtained more recently in Refs. 25 and 29.

One can see that the above experimental data fit well the theoretical predictions and, in particular, the expressions (10) for $\Gamma_{f,s}$. The experimental activation energies ε_f and ε_s have to be identified with ε_h and ε_e^T, respectively.

IV. HIGH-TEMPERATURE RECORDING

A. Characteristic field amplitudes

The recording stage corresponds to $F_K \neq 0$ and zero initial conditions for N_K^+ and H_K in Eqs. (5). Using the standard Laplace transformation, one can easily find the dependences $N_K^+(t)$ and $H_K(t)$ and calculate then the field amplitude $E_K(t)$ from Eq. (7). As follows from the structure of Eqs. (5) and the results of Sec. III, the amplitude E_K may be represented in the form

$$E_K = E_f(1-e^{-\Gamma_f t}) + E_s(1-e^{-\Gamma_s t}), \tag{14}$$

where E_f and E_s are the components of the stationary amplitude $E_K(\infty)$, related to the f and s processes. The component E_f may be named the quasistationary amplitude because this is the value of $E_K(t)$ achieved, actually, by the end of the fast stage and varying afterwards very slowly. The components $E_{f,s}$ have to be calculated in the leading approximation in $\xi_{e,h}$. The final result for $E_{f,s}$ and $E_K(\infty)=E_f+E_s$ is

$$E_f = \frac{m}{2} E_{eff} \frac{\gamma_e^{ph}}{\gamma},$$

$$E_s = E_f \frac{(\gamma_h\xi_h - \gamma_e\xi_e)}{\gamma_e(\xi_e+\xi_h)},$$

$$E_K(\infty) = \frac{m}{2} E_{eff} \frac{\gamma_e^{ph}}{\gamma_e} \frac{1}{1+\xi_e/\xi_h}, \tag{15}$$

where $E_{eff}=E_{PV}+iE_D$ is the effective driving field. The relation for E_f has a simple structure and clear meaning. This is the field amplitude resulting from the balance between the diffusion and photovoltaic electronic currents (which are the cause for charge separation) on the one hand and the electronic and protonic Ohmic currents on the other side. The quasistationary amplitude E_f has nothing to do with the subsequent slow process of charge compensation.

The expression for E_s is far from trivial; it requires some comments. In the high-temperature limit, where $\gamma_e^T \gg \gamma_e^{ph}$ and ξ_e is actually real, the amplitude E_s can change its sign as a function of T. Changing the sign of E_s/E_f from positive to negative means that the kinetics of $|E_K|$ changes from monotonous to nonmonotonous with a maximum at $t \simeq \Gamma_f^{-1}$. Using Eqs. (3) and (6), one finds that the critical temperature T_c, defined by the condition $E_s=0$, meets the equation $\gamma_h/H_0=\gamma_e^T/N_t$, which is equivalent to

$$\mu_h = \mu_e n_0^T/N_t \simeq \mu_e \tau_e S_T. \tag{16}$$

The solution to this equation (if it exists in the high-temperature region) depends on neither H_0 nor N_t. It characterizes therefore some fundamental relation between the electronic and protonic conductions. According to our assumptions, $\varepsilon_e^T > \varepsilon_h$. This means that E_s is of the same sign as E_f for $T<T_c$ and of the opposite sign for $T>T_c$.

In order to explain an appreciable amount of accumulated experimental data on LiNbO$_3$ crystals (see below in this and next sections), we take $T_c \simeq 200$ °C. This critical temperature corresponds to the intersection point of the lines 1 and 4 in Fig. 2. Some theoretical justification of the assumption made may be done using the following simple model expressions
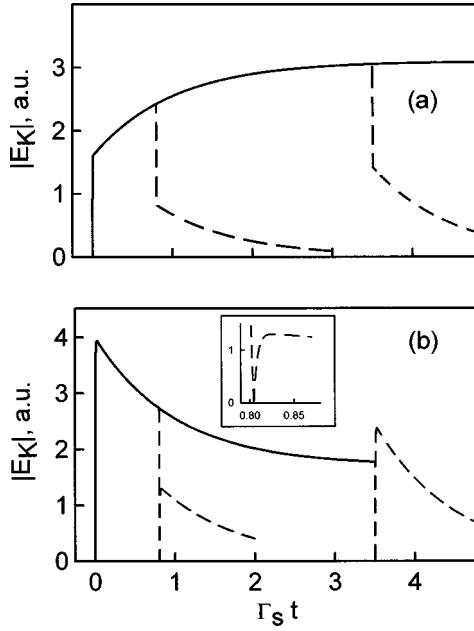
FIG. 4. Kinetic plots of $|E_K(t)|$ in the high-temperature region, $\gamma_e^T \gg \gamma_e^{ph}$. The crystal parameters are the same as for Figs. 2 and 3. (a) $T < T_c$, $\gamma_e^T H_0 = \gamma_h N_t/2$. The solid curves correspond to recording and the dashed ones to the following relaxations for two different recording times. Details of the f stages cannot be resolved with this time scale. (b) The same for $T > T_c$, $\gamma_e^T H_0 = 3 \gamma_h N_t$; the inset shows in detail the f stage of the first relaxation process.

for n_e^T and μ_e: $n_e^T = N_D \exp(-\varepsilon_n/k_B T)$ and $\mu_e = \mu_e^0 \exp(-\varepsilon_\mu/k_B T)$, where $\varepsilon_n + \varepsilon_\mu = \varepsilon_e^T$. With these expressions we have, from Eq. (16),

$$T_c = \frac{\varepsilon_e^T - \varepsilon_h}{k_B \ln(\mu_e^0/\mu_h^0)}. \tag{17}$$

If we take $\varepsilon_e^T - \varepsilon_h = 0.2$ eV, we find out that the temperature $T_c = 200$ °C corresponds to the ratio of the mobility preexponential factors $\mu_e^0/\mu_h^0 \approx 10^2$, which is consistent with the microscopical models of electron and ion transport.

Figures 4(a) and 4(b) illustrate the kinetics of $|E_K|$ for $T < T_c$ and $T > T_c$. The f and s stages of recording are well pronounced. The change in $|E_K|$ is relatively small (and comparatively slow) during the s stage. In this connection the quasistationary value E_f is sometimes mistaken for the stationary one in experimental studies.

Let us turn to experimental facts on the recording process supporting our value of T_c. The occurrence of slow and fast stages of high-temperature recording in LiNbO$_3$ crystals was recognized early.[3,7] It was found for $T = 176–180$ °C that after a fast initial saturation of the amplitude $|E_K|$ its slow growth persists. Unfortunately, experiments in this temperature region were hampered by fluctuations of the position of the light fringes during long-term recording. Measurements in the high-temperature region $T = 180–300$ °C have been performed more recently.[17] They have shown that for $T > 230$ °C, the field amplitude $|E_K|$ experiences a pronounced maximum after the f stage, whereas below 200 °C this peculiarity is absent.
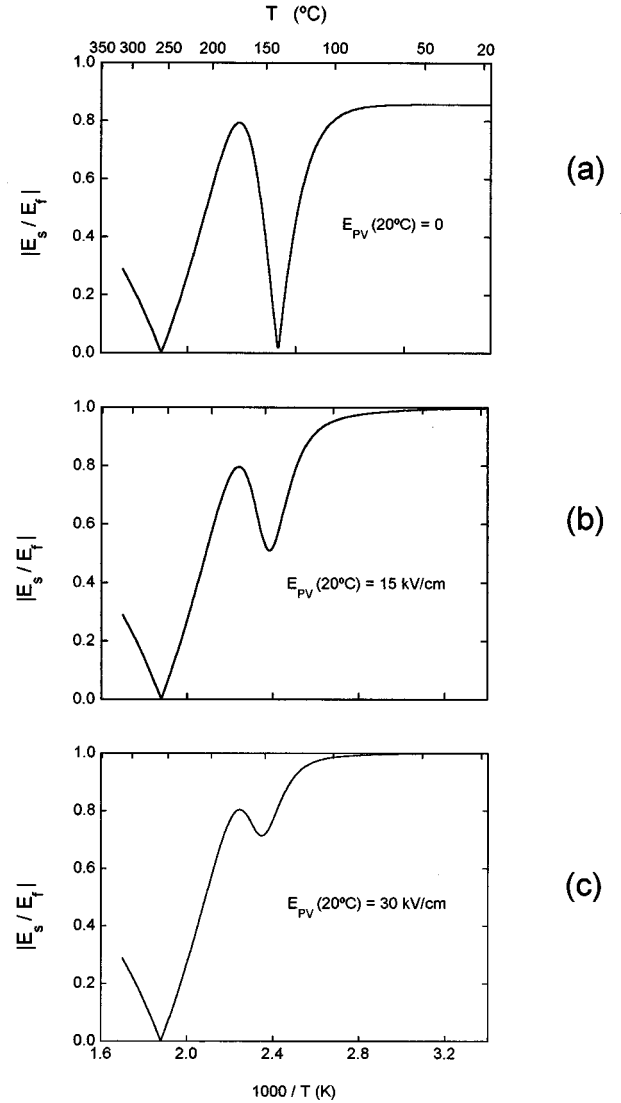

FIG. 5. Temperature dependences of the ratio $|E_s/E_f|$, characterizing the f and s recording stages, for three different values of the photovoltaic field at room temperature.

Figure 5 shows the temperature dependences of the ratio $|E_s/E_f|$, given by Eqs. (15), for three representative values of the photovoltaic field at room temperature. One sees that irrespectively of the value of E_{PV} this ratio turns to zero at $T = T_c \simeq 200$ °C, which corresponds to the above-discussed high-temperature peculiarities of the recording kinetic. The second noticeable minimum at $T \simeq 140$ °C is pronounced only for a sufficiently weak photovoltaic effect. At this minimum we have $H_0 \gamma_e^{ph} \simeq N_t \gamma_h$. For $T \lesssim 100$ °C the ratio $|E_s/E_f|$ is near 1.

In the temperature region where $\gamma_e^T \ll \gamma_e^{ph}$ ($T \lesssim 150$ °C in Fig. 2), Eqs. (14) and (15) admit oscillations of $|E_K(t)|$ during the s stage of recording. These oscillations are pronounced for $E_{PV} \gg E_D$; their relative amplitude depends strongly on T (see Fig. 6). This temperature dependence correlates with the dependence $|E_s/E_f|(T)$ in Fig. 5. We do not know of any experimental confirmation of this prediction of the theory. The main difficulty for the detection of the photovoltaic oscillations comes from their low frequency.
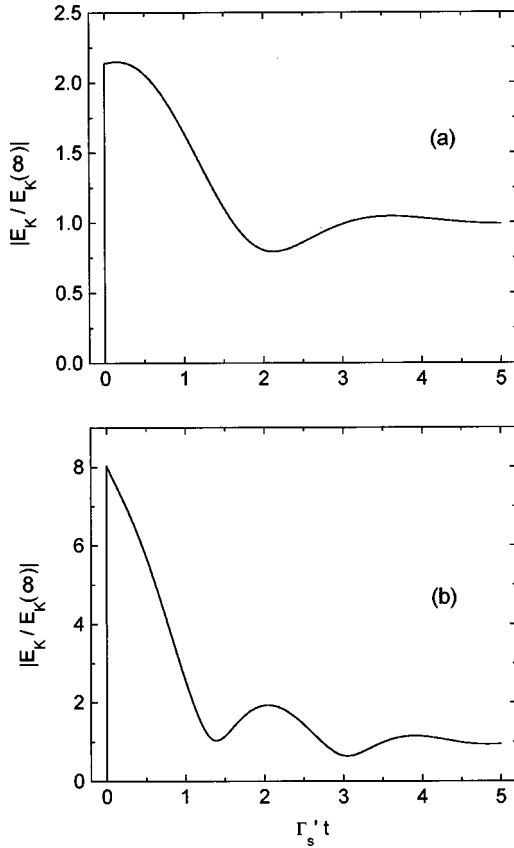
FIG. 6. Oscillations of $|E_K(t)|$ during the s stage of recording caused by the photovoltaic effect. The crystal parameters are the same as for Figs. 2 and 3, and $E_{\mathrm{PV}}(20\,°\mathrm{C})=70\,\mathrm{kV/cm}$. Cases (a) and (b) refer to $T=152$ and $135\,°\mathrm{C}$, respectively.

B. Charge compensation

In fact, the above results on the field amplitude do not fully characterize the recording process. An important piece of information concerning the amplitudes of electronic and protonic gratings is still missing. We refer to N_K^+ as the amplitude of electronic grating because the spatial modulation of N^+ is produced by trapped electrons.

To characterize the amplitudes N_K^+ and H_K, we decompose them into f and s parts by analogy with Eq. (14) for E_K:

$$N_K^+ = N_f^+(1-e^{-\Gamma_f t}) + N_s^+(1-e^{-\Gamma_s t}),$$

$$H_K = H_f(1-e^{-\Gamma_f t}) + H_s(1-e^{-\Gamma_s t}). \tag{18}$$

The corresponding components of the stationary amplitudes, $N_{f,s}^+$ and $H_{f,s}$, are coupled with each other by the relations obtained in Sec. III: $N_f^+\gamma_h = H_f\gamma_e$ and $H_s = -(1+\xi_e\gamma_e/\gamma - \xi_h\gamma_h/\gamma)N_s^+ \simeq -N_s^+$. Furthermore, one can find out algebraically from Eqs. (5), (8), and (18) that $N_f^+ \simeq N_s^+\Gamma_s\gamma_e/\Gamma_f\gamma_h$ and $H_f \simeq -H_s\Gamma_s/\Gamma_f$. Obviously, we have $|H_f|,|N_f^+| \ll |H_s| \simeq |N_s^+|$. This means that sufficiently long recording results in nearly complete compensation of electron and proton charges, $H_K \simeq -N_K^+$. Such a charge compensation is the essence of fixing during recording.

The value of the compensated (hidden) charge is an important characteristic of the recording process. It defines, as

we shall see in Sec. V, the characteristic features of the subsequent relaxation processes. Assuming that the recording process is long enough to produce a strong charge compensation, we obtain, in the leading approximation in $\xi_{e,h}$ for the value of compensated charge,

$$H_K \simeq -N_K^+ \simeq i\,\frac{m}{2}\,N_t\,\frac{\gamma_e^{\mathrm{ph}}}{\gamma_e}\,\frac{E_{\mathrm{eff}}}{E_q}\,\frac{(1-e^{-\Gamma_s t})}{\xi_e+\xi_h}. \tag{19}$$

As for the value of noncompensated charge, $N_K^+ + H_K$, it is fully characterized by Eqs. (7), (14), and (15).

Now we specify the expression ''sufficiently long recording time.'' Using Eqs. (18) and the above relations for $N_{f,s}^+$, we find out easily that the condition for strong charge compensation, $|N_K^+ + H_K| \ll |N_K^+|, |H_K|$, is fulfilled for the recording time $t \gg \gamma_h^{-1}$. The asymmetry between electrons and protons stems from the fact that protons are optically passive. In the temperature region where $\gamma_e^{\mathrm{ph}} \ll \gamma_h$ ($T \gtrsim 130\,°\mathrm{C}$ in Fig. 2), the restriction on the recording time is equivalent to the inequality $t \gg \Gamma_f^{-1}$. In the opposite case $\gamma_e \simeq \gamma_e^{\mathrm{ph}} \gg \gamma_h$ ($T \lesssim 100\,°\mathrm{C}$ in Fig. 2), the recording time t, needed to reach the compensation, is much longer than γ_h^{-1}, which, in turn, is much longer than the duration of the f stage of recording, Γ_f^{-1}. This restriction on t is very hard for experiment.

The overall picture of charge separation during recording looks now fairly simple. During the fast stage, which ends up by $t \simeq (2-3)\Gamma_f^{-1}$ without any strong charge compensation, the field amplitude E_K approaches its quasistationary value E_f. The subsequent long and slow evolution of $E_K(t)$ is accompanied by the accumulation of the ''hidden'' charges; this accumulation saturates only for $t \gtrsim (\Gamma_s')^{-1} \gg \Gamma_f^{-1}$. The change of E_K during the s stage is exclusively due to a noncomplete charge compensation for the s mode; see Eqs. (13). This change is proportional to the sum $N_s^+ + H_s$, i.e., to the combination $\gamma_h\xi_h - \gamma_e\xi_e$. This explains the structure of the expression (15) for E_s. It should be remembered that the dependence $|E_K(t)|$ may look apparently saturated after the f stage of recording (see Figs. 1 and 2): however, the accumulation of the compensated charges still persists.

Let us analyze finally the temperature dependence of the maximum value of compensated charge, which is achieved at the end of the s stage of recording. In the high-temperature limit $\gamma_e^T \gg \gamma_e^{\mathrm{ph}}$, we have, for $\Gamma_s t \gtrsim 2-3$,

$$|H_K(\infty)| \simeq \frac{m}{2}\,\frac{\gamma_e^{\mathrm{ph}}}{\gamma_e^T}\,\frac{|E_{\mathrm{eff}}|}{E_D}\,\frac{N_t H_0}{N_t+H_0}. \tag{20}$$

This value, as well as the expression for $|E_K(\infty)|$ [see Eqs. (15)], includes the factor $\gamma_e^{\mathrm{ph}}/\gamma_e^T$, sharply decreasing with increasing T. In the low-temperature limit, where $\gamma_e^{\mathrm{ph}} \gg \gamma_e^T$, we have $|H_K(\infty)| \simeq mN_t/2$, which is much higher than the value given by Eq. (20). Curves 1 and 2 in Fig. 7 illustrate the temperature dependence of the ratio $2|H_K(\infty)|/mN_t$ for $E_{\mathrm{PV}}=0$ and $E_{\mathrm{PV}}(20\,°C)=60\,\mathrm{kV/cm}$, respectively. It is seen that the positive influence of the photovoltaic effect is noticeable, but not very strong. A sharp decrease for $T \gtrsim 170\,°\mathrm{C}$ remains the most prominent feature of curves 1 and 2. Curve 3 in Fig. 7 is plotted for $E_{\mathrm{PV}}(20\,°C) = 60\,\mathrm{kV/cm}$ and neglecting thermal electrons. The decrease of $|H_K(\infty)|$ in the high-temperature region is comparatively
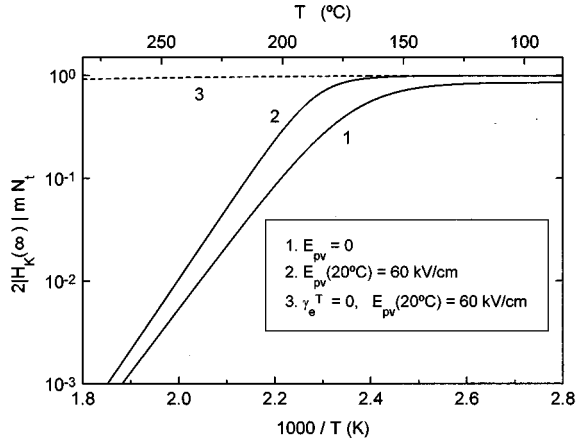
FIG. 7. Temperature dependences for the amplitude of the protonic grating $H_K(\infty)$. Curves 1 and 2 are plotted for the photovoltaic field $E_{PV}(20\,°C)$ equal to 0 and 60 kV/cm, respectively, and the previous values of the crystal parameters. Curve 3 is obtained for $\gamma_e^T = 0$ and $E_{PV}(20\,°C) = 60$ kV/cm.

weak in this latter case. The difference between curves 1,2 and curve 3 makes clear the negative impact of the thermal excitation on high-temperature recording. The fact of a strong decrease of the efficiency of recording for $T \gtrsim 170\,°C$ is known from experiment[3,17] and provides additional support for our model.

It should be emphasized that decreasing temperature not only results in increasing the stationary amplitude $H_K(\infty)$, but also in drastically increasing the time $1/\Gamma'_s$ needed to build up the protonic grating; see, e.g., Fig. 3. For this reason some trade-off should be between the high value of accumulated charge and a reasonably short recording time. Experiment shows that the optimum temperature for fixing is about 170 °C in the case of LiNbO$_3$,[3,17] which is in harmony with our theory.

V. RELAXATION PROCESSES

A. General observations

The recording stage is followed by relaxation processes. These proceed in spatially homogeneous conditions [zero effective driving force F_K in Eqs. (5)], either in the dark or under a uniform illumination. It is clear that any relaxation process consists of f and s stages. The field amplitude $E_K(t)$ may, then, be represented in the form

$$E_K = E_f e^{-\Gamma_f t} + E_s e^{-\Gamma_s t}. \tag{21}$$

Analogous expressions [with the amplitudes $N_{f,s}^+$ and $H_{f,s}$ coupled by Eqs. (13)] are valid for $N_K^+(t)$ and $H_K(t)$.

The s stage of any relaxation process always means decay of the field amplitude. After completion of this stage any spatial inhomogeneity of the charge distribution has disappeared. As concerns the fast stage of relaxation, it can result in a decrease (decay), as well as in an increase of the amplitude E_K. The developing process is the best known and important example of the fast stage of relaxation. Developing means a considerable increase of the field amplitude under uniform illumination because of deterioration of the charge compensation reached after recording; see segments 2–3 and

4–5 in Fig. 1(a). Often, developing experiments are performed at room temperature after a high-temperature fixing procedure.

The term decay is usually referred to decreasing amplitude $|E_K|$ during relaxation (fast or slow). The decay may occur under illumination or in the dark, and it is depicted by segments 3–4 and 5–6 in Fig. 1(a) and segments 1–2 and 3–4 in Fig. 1(b). The reciprocal rate of slow relaxation $\Gamma_s^{-1}(T)$, taken in the dark, characterizes the storage time of the fixed holograms as a function of the temperature. This time is much longer than the dielectric relaxation time, $\gamma^{-1} = \Gamma_f^{-1}$.

In contrast to the s stage of recording, the amplitude $|E_K(t)|$ cannot experience any oscillations during the s stage of decay under illumination in spite of the presence of an imaginary part of Γ_s. It is so because $|E_K| \propto \exp(-\Gamma_s' t)$ at this stage.

Let us suppose that the initial values $N_K^+(0)$ and $H_K(0)$ [and consequently $E_K(0)$] are known for a certain relaxation process. In this case, in addition to the values of the corresponding relaxation rates $\Gamma_{f,s}$, the field amplitude E_s, achieved after the fast stage ($\Gamma_f t \simeq 2-3$), is the most important observable characteristic of the process under study. This amplitude corresponds to the points 3, 4, and 5 in Fig. 1(a) and to the points 1 and 3 in Fig. 1(b). It depends generally on the initial conditions and the type of relaxation process.

Using Eqs. (13) to link H_f with N_f^+ and H_s with N_s^+, the obvious conditions $H_K(0) = H_f + H_s$ and $N_K^+(0) = N_f^+ + N_s^+$, and Eq. (7), we get the following general relations:

$$N_s^+ = \frac{\gamma_h N_K^+(0) - \gamma_e H_K(0)}{\gamma},$$

$$E_s = iE_q \frac{(\gamma_h \xi_h - \gamma_e \xi_e)}{\gamma} \frac{N_s^+}{N_t}. \tag{22}$$

The values of $\gamma_{e,h}$ and $\xi_{e,h}$ correspond to the relaxation process under study.

The case of strong charge compensation in the initial state $[N_K^+(0) \simeq -H_K(0)]$ is worthy of particular attention. We have here $N_s^+ \simeq N_K^+(0)$ and

$$E_s \simeq iE_q \frac{(\gamma_h \xi_h - \gamma_e \xi_e)}{\gamma} \frac{N_K^+(0)}{N_t}. \tag{23}$$

Equation (23) shows that a relatively small variation of $N_K^+(0)$ [and $H_K(0)$] gives rise to a small correction of E_s. The corresponding change in the initial field amplitude $E_K(0)$ (which is defined by the initial value of noncompensated charge) can, however, be very strong. As for the above relation for N_s^+, it is quite obvious, because the amplitudes N_K^+ and $H_K \simeq -N_K^+$ decrease considerably only during a long time comparable with the value $1/\Gamma_s'$ for the slow relaxation process. During the f stage of relaxation, the compensated (coupled) charges experience no noticeable degradation.

As follows from these observations, we can use the same initial condition to describe the f stage of a new relaxation process which follows the considered one. The number of fast relaxation cycles sufficient to decrease $N_K^+(0)$ may be

estimated as Γ_f / Γ'_s, which is much greater than 1, especially in the low-temperature region; see Fig. 3.

The amplitudes N_K^+ and H_K attained during the high-temperature recording for $t \gg \Gamma_f^{-1}$ satisfy fully the requirement $N_K^+(0) \simeq -H_K(0)$ imposed on the initial conditions for relaxation. If the initial amplitudes $N_K^+(0)$ and $H_K(0)$ are not nearly opposite, they acquire this property after the f stage of the first relaxation process. An important example is fixing by means of recording at a low temperature with subsequent heating of the sample. The s stage of recording is not available at low temperatures, which means the absence of charge compensation. The subsequent f stage of dark decay at an elevated temperature produces such a compensation.

The general view of fast relaxation processes is now fairly simple. If we have initially a fixed grating with strongly compensated electron and proton charges, the field amplitude E_s attained after the f stage of a certain subsequent relaxation process is defined by the conditions of this process, or more precisely, it is determined by the value of the parameter $\xi_h \gamma_h / \gamma - \xi_e \gamma_e / \gamma$ for the corresponding s mode. Therefore, repetition of a sequence of fast relaxation processes results in repetition of the corresponding values of E_s. A considerable degradation of fixing occurs after many relaxation cycles. This essential feature of fixed holograms has been demonstrated experimentally.[29,33]

Below we apply the general equation (23) to particular relaxation processes, depicted in Fig. 1, and discuss the relation between the theory and experiment.

Since the conditions for recording, developing, and decay processes are often different, we use in what follows, when necessary, the indices ''rec,'' ''dev,'' ''dark,'' and ''light'' to specify the process under study and its conditions.

B. High-temperature relaxation

Let us consider the relaxation in the high-temperature limit, where $\gamma_e^{ph} \ll \gamma_e^T$, γ_h ($T \gtrsim 160\,°C$ in Fig. 2). In this limit, a considerable lowering of the operating temperature is hardly possible during a time shorter than the longest characteristic time of the charge relaxation, $1/\Gamma'_s$. For this reason we restrict ourselves to the same temperature for both the recording and relaxation processes. The value E_s for the relaxation process is nearly the same here in the dark and under light:

$$E_s \simeq i E_D \frac{\gamma_h N_t - \gamma_e^T H_0}{N_t H_0 (\gamma_h + \gamma_e^T)} N_K^{rec}. \qquad (24)$$

The sign of this expression coincides with the sign of the component E_s^{rec}, characterizing the s stage of recording. This means that the grating amplitude $E_K(t)$ changes its sign during the f-relaxation stage for $T > T_c$ (see Sec. IV) and remains of the same sign for $T < T_c$. In other words, the peculiarity of recording for $T > T_c$ should correlate with the peculiarity of the f relaxation following the recording. This is illustrated by Figs. 4(a) and 4(b). The predicted nontrivial features of high-temperature behavior are in excellent agreement with experiment.[17] This is one more piece of evidence for the participation of the thermal electrons in fixing-related photorefractive phenomena in $LiNbO_3$.
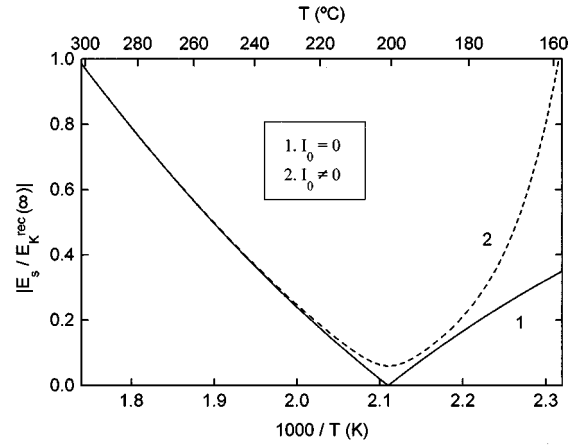

FIG. 8. Temperature dependences of the ratio $|E_s / E_K(\infty)|$ for dark (solid curve) and light-induced (dashed curve) relaxations at $T = T_{rec}$. The photovoltaic field $E_{PV}(20\,°C)$ is 60 kV/cm.

It is important to realize that the slow component $E_s(t_{rec})$, together with N_K^{rec}, experiences saturation only for $(\Gamma_s t)_{rec} \gtrsim 1$. At the same time, the amplitude E_K^{rec} reaches its quasistationary level E_f, already for $(\Gamma_f t)_{rec} \gtrsim 2-3$. This means that the fraction of the s component of the relaxation, E_s / E_K^{rec}, grows strongly with t_{rec}. Mostly the f component has to be present in the relaxation after an insufficiently long recording; see also Fig. 3. Qualitatively, these features correspond to experimental data of Refs. 3 and 23.

In the case of a stationary recorded grating $\exp(\Gamma_s t)_{rec} \gg 1$, we have in the general case

$$\frac{E_s}{E_K^{rec}(\infty)} = \frac{\gamma_h}{\gamma} - \frac{\gamma_e}{\gamma} \frac{\xi_e}{\xi_h}. \qquad (25)$$

This expression gives the maximum possible value of $|E_s / E_K^{rec}|$ for the temperature T. For $H_0 \gg N_t$ and $\gamma_e^T \gtrsim \gamma_h \gg \gamma_e^{ph}$ this ratio may exceed 1 in absolute value. This means that point 3 in Fig. 1(b) may be higher than point 2.

Figure 8 shows the ratio $|E_s / E_K^{rec}(\infty)|$ as a function of T within the interval $160-300\,°C$ for dark and light-induced relaxations and the previous values of the representative parameters. In the first case, the ratio $E_s / E_K^{rec}(\infty)$ is real and it changes its sign from positive to negative with increasing t, in full agreement with Eq. (24). In the second case, this ratio is complex because of the photovoltaic contribution to ξ_e. For $T \gtrsim 170\,°C$ this contribution is relatively small. It results, however, in the replacement of the zero minimum value of $|E_K(t)|$ during the f stage of relaxation [see Fig. 4(b)] by a small finite one. Starting from $T \simeq 175\,°C$, the function $|E_s / E_K^{rec}(\infty)|(T)$, given by curve 2, grows rapidly with decreasing T owing to an increasing imaginary part of ξ_e. The rate of this growth depends, of course, on the value of the photovoltaic field.

C. Developing

This process refers to the fast stage of light-induced relaxation at a low temperature. Let T_{rec} lie in the intermediate-temperature region defined by inequalities $T_{rec} < T_c$ and $\gamma_{ph}(T_{rec}) \ll \gamma_e^T(T_{rec})$. This region is presumably $170-180\,°C$
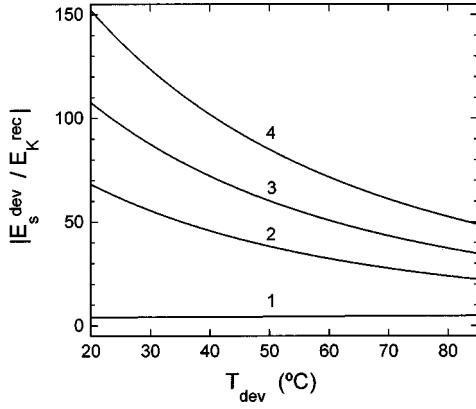
FIG. 9. Dependence of $|E_s^{\mathrm{dev}}/E_K^{\mathrm{rec}}|$ on the developing temperature for a grating fixed previously up to the saturation at $T_{\mathrm{rec}}=170$ °C. Curves 1, 2, 3, and 4 are plotted for $E_{\mathrm{PV}}(20$ °C) equal to 0, 12, 30, and 60 kV/cm, respectively.

and it is near the optimum for the fixing procedure in LiNbO$_3$. The developing temperature T_{dev} is supposed to be much lower than T_{rec} so that $\gamma_e^{\mathrm{ph}}(T_{\mathrm{dev}}) \gg \gamma_e^T(T_{\mathrm{dev}}), \gamma_h(T_{\mathrm{dev}})$; see also Fig. 2. In this case, we have from Eq. (23) the following simple relation:

$$E_s^{\mathrm{dev}} \simeq E_{\mathrm{eff}}^{\mathrm{dev}} \frac{H_K^{\mathrm{rec}}}{N_t}. \tag{26}$$

It has been assumed that the grating amplitudes H_K^{rec} and $(N_K^+)^{\mathrm{rec}}$ do not experience considerable changes during cooling the crystal down from T_{rec} to T_{dev}. According to Eq. (19), the ratio H_K^{rec}/N_t is

$$\frac{H_K^{\mathrm{rec}}}{N_t} \simeq i \frac{m}{2} \frac{H_0}{H_0+N_t} \left(\frac{\gamma_e^{\mathrm{ph}}}{\gamma_e^T} \frac{E_{\mathrm{eff}}}{E_D} \right)_{\mathrm{rec}} (1-e^{-\Gamma_s t})_{\mathrm{rec}}. \tag{27}$$

In accordance with this expression, a pronounced increase of E_s^{dev} as a function of t_{rec} takes place for LiNbO$_3$ crystals doped with Fe and Cu.[3,8]

Let us find now the ratio $|E_s^{\mathrm{dev}}/E_K^{\mathrm{rec}}|$, which characterizes the value of the jump from point 2 to 3 in Fig. 1(a). Assuming a steady state for E_K^{rec} (and H_K^{rec}) and using Eq. (15) for $E_K(\infty)$, one obtains the following explicit expression:

$$\left| \frac{E_s^{\mathrm{dev}}}{E_K^{\mathrm{rec}}} \right| \simeq \frac{|E_{\mathrm{eff}}^{\mathrm{dev}}|}{E_D^{\mathrm{rec}}} \frac{H_0}{N_t}. \tag{28}$$

In the low-temperature region, usually $E_{\mathrm{eff}}^{\mathrm{dev}} \simeq E_{\mathrm{PV}}^{\mathrm{dev}} \gg E_D^{\mathrm{dev}}$; on the other hand, the diffusion field $E_D^{\mathrm{rec}}=Kk_BT_{\mathrm{rec}}/e$ is not much larger than E_D^{dev}. Since $H_0 \gtrsim N_t$ in LiNbO$_3$, we have $|E_s^{\mathrm{dev}}| \gg |E_K^{\mathrm{rec}}|$. In such a way, the field amplitude should experience a considerable increase during development. This characteristic feature has been observed in many experiments.[3,7,29,34]

Figure 9 illustrates the temperature dependence of $|E_s^{\mathrm{dev}}/E_K^{\mathrm{rec}}|$ for different values of $E_{\mathrm{PV}}(20$ °C) on the basis of Eq. (28). The decrease in E_s^{dev} with decreasing temperature comes here from the decrease of $E_{\mathrm{PV}}(T)$. Recall that the ratio $E_s^{\mathrm{dev}}/E_K^{\mathrm{rec}}$ becomes smaller by a factor $1-\exp(\Gamma_s t)_{\mathrm{rec}}$ if the s stage of the recording process is not finished.

Decreasing T_{rec} results in a sharp decrease of Γ_s'. Completion of the s stage of the recording process (fixing of the hologram) may become problematic for this reason.

D. Low-temperature decay

The process under study is the decrease of the field amplitude E_K in the dark or under a uniform illumination (see, e.g., segments 3–4 and 5–7 in Fig. 1). We restrict ourselves to the same low-temperature region as in Sec. V C, $\gamma_e^{\mathrm{ph}}(T_{\mathrm{dec}}) \gg \gamma_e^T(T_{\mathrm{dec}}), \gamma_h(T_{\mathrm{dec}})$.

Let us assume first that the low-temperature relaxation proceeds in the dark. In this case some decay of the grating amplitude takes place during the f stage. Using Eqs. (15) and (23), one can obtain for the case of stationary recording, $(\Gamma_s t)_{\mathrm{rec}} \gtrsim 2-3$,

$$\frac{E_s^{\mathrm{dec}}}{E_K^{\mathrm{rec}}} \simeq \frac{T_{\mathrm{dec}}}{T_{\mathrm{rec}}}. \tag{29}$$

Hence some small drop from point 2 to 4 in Fig. 1(a) is determined in this case only by the temperature ratio.

It is useful also to link the amplitudes E_s^{dec} and E_s^{dev}. Their ratio does not depend on the recording time and can be represented in the form

$$\frac{E_s^{\mathrm{dev}}}{E_K^{\mathrm{dec}}} \simeq i \frac{H_0}{N_t} \frac{E_{\mathrm{eff}}}{E_D}. \tag{30}$$

The right-hand side of this expression is supposed to be taken at the temperature $T_{\mathrm{dec}}=T_{\mathrm{dev}}$. Hence we have, as expected, $|E_s^{\mathrm{dev}}| \gg |E_s^{\mathrm{dec}}|$. Since the ratio $T_{\mathrm{dec}}/T_{\mathrm{rec}}$ varies within a narrow range of $\simeq 0.65-0.8$, the dependence $|E_s^{\mathrm{dev}}/E_s^{\mathrm{dec}}|$ on T_{dec} is not much different from the one given by Eq. (28) and illustrated by Fig. 9.

The s stages of the relaxation processes following the f stage of dark decay or developing both result in decay of the remaining grating to zero; see the segments 4–8 and 5–7 in Fig. 1(a). The rates of the corresponding relaxations in the dark and under light are given by Eqs. (10) and (11) for Γ_s and Γ_s', respectively. According to our model, we have $(\Gamma_s')_{\mathrm{light}} \gg \Gamma_s^{\mathrm{dark}}$. This feature was clearly seen in experiments with LiNbO$_3$ crystals carried out for $T_{\mathrm{dec}} \simeq 80-90$ °C.[29,33]

The s stage of the light-induced decay [see segment 5–6 in Fig. 1(a)] may be interrupted at a certain time moment by switching off the uniform illumination. We return in this case to the f stage of dark decay, that is, to a short-time increase of the relaxation rate. The value of the corresponding drop of the amplitude $|E_K|$ is obviously relatively small. Just this enhancement of the relaxation rate by means of removing illumination was detected recently in Ref. 33. This feature was not, however, explained properly.

Let us finally recall that the relation between the s and f components of E_K for a decay process depends significantly on the recording time. In the case of a short recording time $(\Gamma_s t)_{\mathrm{rec}} \ll 1$, the decay consists mainly of the f stage. This feature is illustrated by Fig. 4(a).

In many experiments $|E_s^{\mathrm{dec}}|$ is much less than $|E_K^{\mathrm{rec}}|$.[23,24,33] This means that the initial process of high-temperature fixing was far from saturation.

VI. DISCUSSION

The presented theory has several remarkable features, which distinguish it from most previous studies. We have used at a high degree the presence of small physical parameters, which determine the character of high-temperature photorefractive processes in LiNbO$_3$ crystals. It has made it possible to focus our attention on key features of these processes and to describe them by fairly simple and general relations.

Among the notions used, the most important one is the separation of the high-temperature processes into fast and slow components. Systematic exploiting of this concept has allowed us to characterize in detail the corresponding fast and slow relaxation rates and to describe in a simple and general manner the characteristic grating amplitudes.

A remarkable feature of our treatment is that it is applied to a wide temperature region, which includes not only the temperatures relevant for the fixing phenomenon, but also the high-temperature domain $T \gtrsim 200\,°C$. Entering in this domain has enabled us to reveal the competitive role of thermal electrons in fixing-related processes and to find distinctive manifestation of these electrons in the kinetics of recording and subsequent relaxation processes.

We have used the whole spectrum of available experimental data on high- and low-temperature photorefractive effects in LiNbO$_3$ to compare them with the predictions of our theory. The main result of such a comparison is a surprisingly good qualitative agreement for a variety of characteristic features of recording, developing, and decay processes. This comparison has allowed us to estimate the parameters which determine the contribution of thermal electrons to charge transport in LiNbO$_3$.

Considerations of different aspects of high-temperature photorefractive phenomena have made it certain that the present level of measurements is still insufficient for a detailed comparison between theory and experiment. Especially this applies to the recording stage. In fact, the requirement of stability of the interference light fringes during the slow stage of recording (which may last many hours) is very hard for most experimental setups. Special provisions have to be taken to avoid strong distortions and noise because of slow thermal and mechanical fluctuations and air convection. There is real hope that implementation of the technique for active stabilization of the light fringes[45] in combination with a vacuum chamber will permit reliable and repeatable recording experiments.[46]

Our analysis of the different processes encourages us to touch the problem of the storage time of a fixed hologram. Many conflicting judgements have been made to clarify this practically important matter; see, e.g., Refs. 2, 25, 32, and 33. Within our model this storage time is nothing else than the rate of slow relaxation, Γ_s^{-1}, taken in the dark. At room temperature this time may be several orders of magnitude longer than the dielectric relaxation time Γ_f^{-1}. For the grating spacing $\Lambda = 1\,\mu m$, $T = 20\,°C$, $N_t = 5 \times 10^{17}\,cm^{-3}$, and the data of Fig. 2, the storage time exceeds 10^3 yr.

The mentioned conflicting estimations could be due to an erroneous identification of the storage time with Γ_f^{-1}. This misinterpretation may have its roots in a insufficiently long duration of the fixing procedure, which, in turn, is caused by fluctuations of the position of the light fringes. As we have seen, the dark decay exhibits mainly the f stage in this case. An extrapolation of the data for the apparent decay rate to room temperature has nothing to do in this case with the storage time.

The last point to discuss is at what extent the above theory may be applied to other photorefractive materials. The approximations used and the general relations obtained remain valid for many photorefractive ferroelectrics like LiTaO$_3$, KNbO$_3$, and BaTiO$_3$. Except for LiNbO$_3$ and LiTaO$_3$ crystals, the photovoltaic transport may be regarded as unimportant, which simplifies the theory. As concerned the particular features associated with the thermo activation dependences of γ_h, γ_e^T, and γ_e^{ph}, they may vary considerably in different cases.

VII. CONCLUSIONS

Our analytical theory based on the conventional two-species equations for charge transfer in LiNbO$_3$ and the systematic use of small physical parameters allows for a simple and general description of a variety of photorefractive phenomena in the wide temperature region 20–300 °C. Thermally excited electrons are shown to be responsible, not only for the dark decay of the recorded information, but also for distinctive features of the recording and relaxation process above 200 °C. A good qualitative agreement between the theory and experiment is obtained for a wide spectrum of characteristics of fixing-related phenomena in LiNbO$_3$. Stabilized long-term experiments are needed to reveal fully the potential of the thermal fixing for applications.

[1] J. J. Amodei and D. L. Staebler, Appl. Phys. Lett. **18**, 540 (1971).

[2] D. L. Staebler, W. J. Burke, W. Phillips, and J. J. Amodei, Appl. Phys. Lett. **26**, 182 (1975).

[3] W. Meyer, P. Wurfel, R. Münser, and G. Müller-Vogt, Phys. Status Solidi A **53**, 171 (1979).

[4] E. Krätzig and R. Orlowski, Appl. Phys. **15**, 133 (1978).

[5] V. V. Kulikov and S. I. Stepanov, Sov. Phys. Solid State **21**, 1849 (1979).

[6] H. Vorman, G. Weber, S. Kapphan, and M. Wöhlecke, Solid State Commun. **57**, 543 (1981).

[7] P. Hertel, K. H. Ringhofer, and R. Sommerfeldt, Phys. Status Solidi A **104**, 855 (1987).

[8] R. Sommerfeldt, R. A. Rupp, H. Vorman, and E. Krätzig, Phys. Status Solidi A **99**, K15 (1987).

[9] R. Matull and R. Rupp, J. Phys. D **21**, 1556 (1988).

[10] M. Carrascosa and F. Agulló-López, J. Opt. Soc. Am. B **7**, 2317 (1990).

[11] G. Montemezzani and P. Günter, J. Opt. Soc. Am. B **7**, 2323 (1990).

[12] D. Kirilov and J. Feinberg, Opt. Lett. **16**, 1520 (1991).

[13] L. Arizmendi, P. D. Townsend, M. Carrascosa, J. Baquedano, and J. M. Cabrera, J. Phys.: Condens. Matter **3**, 5399 (1991).

[14] S. Klauer, M. Wöhlecke, and S. Kaphan, Phys. Rev. B **45**, 2786 (1992).

[15] R. Müller, L. Arizmendi, M. Carrascosa, and J. M. Cabrera, Appl. Phys. Lett. **60**, 3212 (1992).

[16] G. Montemezzani, M. Zgonik, and P. Günter, J. Opt. Soc. Am. B **10**, 171 (1993).

[17] M. Carrascosa and L. Arizmendi, J. Appl. Phys. **73**, 2709 (1993).

[18] S. Orlov, D. Psaltis, and R. R. Neurgaoncar, Appl. Phys. Lett. **66**, 2466 (1993).

[19] M. Jeganathan and L. Hesselink, J. Opt. Soc. Am. B **11**, 1791 (1994).

[20] R. Müller, M. T. Santos, L. Arizmendi, and J. M. Cabrera, J. Phys. D **27**, 241 (1994).

[21] A. S. Kewitsch, M. Segev, A. Yariv, G. J. Salamo, T. W. Towe, E. J. Sharp, and R. R. Neurgaonkar, Phys. Rev. Lett. **73**, 1174 (1994).

[22] J. F. Heanue, M. C. Bashaw, and L. Hesselink, Science **265**, 749 (1994).

[23] R. Müller, L. Arizmendi, M. Carrascosa, and J. M. Cabrera, J. Appl. Phys. **77**, 308 (1995).

[24] R. M. Müller, L. Arizmendi, M. Carrascosa, and J. M. Cabrera, Opt. Mater. **4**, 290 (1995).

[25] A. Yariv, S. Orlov, G. Rakuljic, and V. Leyva, Opt. Lett. **20**, 1334 (1995).

[26] J. F. Heanue, M. C. Bashaw, A. J. Daiber, R. Snyder, and L. Hesselink, Opt. Lett. **21**, 1615 (1996).

[27] M. Carrascosa and F. Agulló-Lopez, Opt. Commun. **126**, 240 (1996).

[28] J. M. Cabrera, J. Olivares, M. Carrascosa, J. Rams, R. Müller, and E. Diegues, Adv. Phys. **45**, 349 (1996).

[29] A. Yariv, S. S. Orlov, and G. A. Rakuljic, J. Opt. Soc. Am. B **13**, 2513 (1996).

[30] K. Buse, S. Beer, K. Peithmann, S. Kapphan, M. Gao, and E. Krätzig, Phys. Rev. B **56**, 1225 (1997).

[31] M. C. Bashaw and J. F. Heanue, J. Opt. Soc. Am. B **14**, 2024 (1997).

[32] G. Rakuljic, Opt. Lett. **22**, 825 (1997).

[33] L. Arizmendi, A. Mendez, and J. V. Alvarez-Bravo, Appl. Phys. Lett. **70**, 571 (1997).

[34] A. Mendez and L. Arizmendi, Opt. Mater. **10**, 55 (1998).

[35] A. M. Glass, D. von der Linde, and T. J. Negran, Appl. Phys. Lett. **25**, 233 (1974).

[36] B. Sturman and V. Fridkin, *The Photovoltaic and Photorefractive Effects in Noncentrosymmetric Materials* (Gordon and Breach, Philadelphia, 1992).

[37] E. Krätzig and O. F. Shirmer, *Photorefractive Centers in Electro-Optic Crystals*, Topics in Applied Physics Vol. 61 (Springer-Verlag, Berlin, 1988), p. 131.

[38] L. Solymar, D. J. Webb, and A. Grunnet-Jepsen, *The Physics and Applications of Photorefractive Materials*, Oxford Series in Optical and Imaging Sciences (Clarendon Press, Oxford, 1996).

[39] K. Buse, Appl. Phys. B: Lasers Opt. **64**, 273 (1997).

[40] W. Jösch, R. Munser, W. Ruppel, and P. Würfel, Ferroelectrics **21**, 623 (1978).

[41] V. M. Fridkin, *Photoferroelectrics* (Springer-Verlag, Berlin, 1979).

[42] B. I. Shklovskii and A. L. Efros, *Electronic Properties of Doped Semiconductors* (Springer, New York, 1984).

[43] B. I. Sturman, M. Mann, J. Otten, and K. H. Ringhofer, J. Opt. Soc. Am. B **10**, 1919 (1993).

[44] B. I. Sturman, E. Shamonina, M. Mann, and K. H. Ringhofer, J. Opt. Soc. Am. B **12**, 1642 (1995).

[45] A. A. Freschi and J. Frejlich, J. Opt. Soc. Am. B **11**, 1837 (1994).

[46] S. Breer, K. Buse, K. Peithmann, H. Vogt, and E. Krätzig, Rev. Sci. Instrum. (to be published).